Composites: Part A 156 (2022) 106867

Contents lists available at ScienceDirect

Composites Part A

journal homepage: www.elsevier.com/locate/compositesa

Should the translaminar fracture toughness of laminated composites be represented by the R or the J curve? A comparison of their consistency and predictive capability

P. Maimí *, A. Ortega, E.V. González, J. Costa

AMADE, Escola Politècnica Superior, Universitat de Girona, Girona, Spain

ARTICLE INFO

Keywords:
Translaminar fracture toughness
Composite materials
Fracture mechanics
Size effect law

ABSTRACT

The translaminar fracture toughness of laminated composites can be determined experimentally assuming either linear elastic fracture mechanics (LEFM) or cohesive zone model (CZM) hypotheses. Each theoretical frame is different in terms of complexity and predictive capabilities. To clarify the latter point, we derived the $R(\Delta a)$ (LEFM) and $J(\omega)$ (CZM) curves from a set of published results on over-height compact tension fracture specimens of different sizes. Then, these curves were used to predict the strength of other coupons of the same material (geometrically similar, scaled, open hole and center cracked specimens). Since the idealization of the fracture phenomena in cohesive zone models is more realistic than in LEFM, the fracture property so obtained is more independent from the size of the specimen used to measure it and its predictive capability embraces a wider range of sizes and geometries.

1. Introduction

Crack growth in laminated composite materials involves several damage mechanisms at different scales. For example, fiber failure, matrix cracking and splitting, fiber–matrix debonding and delaminations occur during a translaminar crack growth (Fig. 1 [1] illustrates the damage pattern of a 0^0 ply in a carbon fiber composite). These damage mechanisms account for the material's resistance to crack advance, referred to as fracture toughness.

Fracture toughness is an important property in structural design as it determines the strength of components with stress raisers as notches, holes or slits [2–4]. Tough, or damage tolerant materials are able to largely retain their strength in spite of in-service degradation or manufacturing defects.

The experimental determination of the fracture toughness relies on the assumption of a theoretical frame which dictates the data reduction process. The most common frame is Linear Elastic Fracture Mechanics (LEFM). LEFM assumes small scale bridging, that is, the non-linear zone at the crack tip is very small in comparison to any other relevant dimension of the problem (coupon dimensions, crack length, etc.). It considers that both ℓ_H and ℓ_V in Fig. 1 (characteristic lengths in the specimen plane of the zone where damage spreads) are small. Accordingly, fracture toughness is described by a single parameter: the critical energy release rate (or its equivalent critical stress intensity factor). In many materials, this scalar value increases as the crack grows, defining what is known as the R-curve. In laminated composites, however, the size of the failure process zone may not fulfill the assumption of being small. Several reports assert the limitations of LEFM methods to characterize fracture toughness [5–8]. Some studies proposed enlarging specimen sizes to fulfill the LEFM assumption of a relatively small non-linear zone [9].

On the other hand, the crack bridging concept, or cohesive zone model (CZM), introduced by Barenblatt [10] and Dugdale [11], accounts explicitly for a damage zone length in the direction of the crack propagation. The non-linear zone is defined as a line (Fig. 1), the length ℓ_H is considered explicitly but ℓ_V is still expected to be small. The Cohesive Zone Model relies on the cohesive law, which relates the bridging stresses to the crack opening, $\sigma(\omega)$. The integration of the cohesive stress with respect to the crack opening is equivalent to the J-integral [12]. The cohesive law represents better than a single parameter (as in LEFM) the process of fracture, especially in those materials where dissipation is governed by extrinsic degradation mechanisms [13].

As fracture toughness is a crucial macromechanical property in design, it is convenient to clarify which theoretical frame, LEFM or CZM, has a wider predictive capability; or whether the increased complexity of CZM pays off. This dilemma is even more relevant in modern high fracture toughness materials where several damage mechanisms intervene at different scales (i.e. hierarchical microstructures).

* Corresponding author.
E-mail address: pere.maimi@udg.edu (P. Maimí).

https://doi.org/10.1016/j.compositesa.2022.106867
Received 26 May 2021; Received in revised form 4 February 2022; Accepted 6 February 2022
Available online 13 February 2022

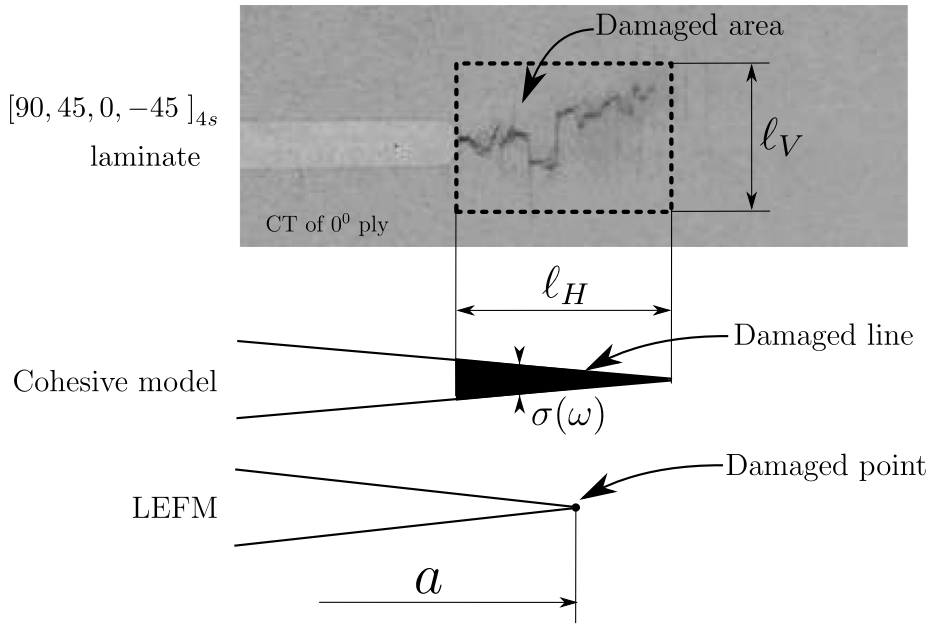

Fig. 1. Computed Tomography (CT) of the damage near the crack tip from Xu et al. [1] and simplifications of the cohesive model and LEFM.

To answer these questions, we took a set of experimental results on fracture specimens (Over-Height Compact Tension) published by researchers from University of Bristol and University of British Columbia [1,14,15] and analyzed the data applying both LEFM and CZM, so that to obtain the R and J curves, respectively. This set of experimental data is particularly useful for the purpose of this work because, in addition to being reported in great detail, it embraces a large range of specimen sizes (specimens scaled up to a factor of 4). As fracture properties, as for any other material property, are expected to be independent of the size of the specimen used to measure it, the experimental results from the scaled specimens represent a validation test for any data reduction procedure [5,16,17]. To check the predictive capability of the R and J curves, we compared the predicted strength of Center Cracked and Open Hole specimens of the same material, and with scale factors up to 16, with the experimental data reported by the same group from Bristol [18,19].

2. Methodology

2.1. Experimental data

This work makes use of a set of experimental results published by Xu et al. [1,14] and Zobeiry et al. [15]. The authors analyzed the translaminar fracture of quasi-isotropic laminates with geometrically similar specimens of different sizes. In particular, we use the results from the Over-height Compact Tension (OCT) tests [1,9,14,15,20–22] to extract the $R(\Delta a)$ and $J(\omega)$ curves. Fig. 2 illustrates the geometry of this specimen.

The compliance of the OCT specimen for quasi-isotropic laminates is approximated from a finite element computation, following the same procedure used by Ortega et al. [23], with the polynomial expression

$$\bar{C} = \left(\frac{1+\bar{a}}{1-\bar{a}}\right)^2 \left(1.489 + 9.9265\bar{a} - 25.633\bar{a}^2 + 39.058\bar{a}^3 - 31.12\bar{a}^4 + 10.305\bar{a}^5\right) \quad (1)$$

where the compliance and crack length are normalized as $\bar{C} = ChE$ and $\bar{a} = a/W$, respectively. h is the specimen thickness and E the Young modulus. This paper also analyzes data from the Open Hole and Centered Crack Tension tests from the same set of publications [1,14,15].

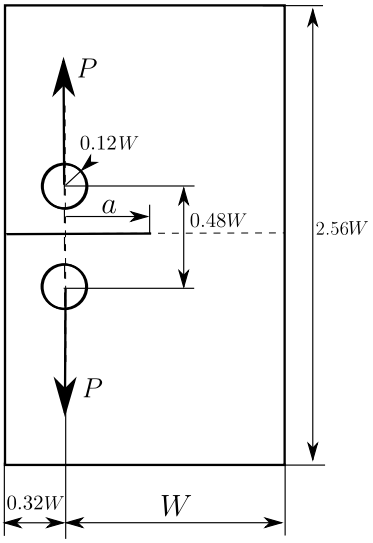

Fig. 2. Over-Height Compact Tension geometry.

Table 1
Laminate properties, where h is the laminate thickness and a_0 the initial notch length.

Stacking	W [mm]	a_0 [mm]	h [mm]	E [MPa]	σ_u [MPa]
$[45, 90, -45, 0]_{4s}$	40.3/80.6/161.2 [14]	0.4 W	4	61 645	990 [24]
$[90, 45, 0, -45]_{4s}$	40.3 [1]/80.6 [15]	0.4 W	4	61 645	990[a]

[a]Property assumed equal to the $[45, 90, -45, 0]_{4s}$ laminate.

The two laminates studied here were made of Hexcel HexPly® IM7/8552 carbon-epoxy pre-preg, with a nominal ply thickness of 0.125 mm. Table 1 gives the laminate stacking sequences, specimen sizes and homogenized properties. More details on the test setup and materials can be found in the Refs. [1,14,15].

The load–displacement curves provided in the cited works were corrected for the compliance of the testing system. That is, the displacements (u_P) reported in the papers [1,14,15] were corrected according to the expression $u = u_P - C_S P$, where C_S is the compliance of the testing system. C_S was found by fitting the linear part of the load–displacement curve to the theoretical compliance of the specimen (defined in Eq. (1)).

2.2. Data reduction for $R(\Delta a)$ and $J(\omega)$ curves

This section describes the methodology followed to obtain the R-curve (based on LEFM assumptions) and the J-curve (CZM) from the same set of load–displacement curves from the OCT tests.

There are several methods to characterize the translaminar fracture of composite laminates. Laffan et al. [25] review methods to obtain the R curve, while Maimí et al. [26] do so for J curves. In this work, we selected methodologies that require only the data provided by the universal testing machine (load and displacement). This decision was taken to follow the easiest experimental methodology and to permit the fairest comparison between both curves (both use the same set of data).

The load displacement curves were idealized with a total of 20 points obtained by a Gaussian average (Fig. 3). We applied the data reduction scheme described below to this set of representative points.

2.2.1. The $R(\Delta a)$ curve

Every method to obtain the R-curve relies on the measurement of the increment of the crack length Δa. This can be done by optical monitoring of the crack front, but this measure is not objective due to the presence of a failure process zone near the crack tip. An alternative, and more objective, method deduces an "apparent" crack length from equaling the experimental compliance to the one defined by the elastic problem in the presence of a sharp crack. Laffan et al. [25] and Bergan et al. [16] compare both methods (optical and compliance) and conclude that, while both methods are acceptable, visual inspection may lead to greater variability in addition to the increased complexity of the test.

In this work, we calculated the compliance for each experimental load displacement point as $C = u/P$. An equivalent crack length resulted from equaling the experimental normalized compliance to Eq. (1). The increment of crack length was then defined as: $\Delta a = \bar{a}W - a_0$.

The Energy Release Rate (ERR) for each experimental point results from the corresponding known load, P, and crack length and the use of the Irwin–Kies equation [25]:

$$G = \frac{P^2}{2h^2 EW}\frac{\partial \bar{C}}{\partial \bar{a}} \tag{2}$$

2.2.2. The $J(\omega)$ curve

The cohesive zone model postulates that the tractions transferred through the crack faces depend on the local separation $\sigma(\omega)$, as sketched in Fig. 1. The integration of the traction separation, or cohesive, law defines the $J(\omega)$ curve:

$$J = \int_0^{\omega} \sigma d\omega \tag{3}$$

The $J(\omega)$ curve defines the amount of energy dissipated per unit surface area to reach a given crack separation, ω.

The most direct method to measure J is by applying its definition as a path integral [12,27]. This is experimentally expensive and prone to scattered results because it requires measuring (usually by Digital Image Correlation) the local displacement field along the path enclosing the failure process zone and the local opening of the crack faces.

Another option is to use a fitting or optimization algorithm that minimizes the deviation between the experimental measurement and the output of a numerical model accounting for the cohesive zone [28–45]. These works differ on the experimental parameters and the algorithm used to obtain the best solution. In this work, we follow the method proposed by Ortega et al. [43,44]. Taking the point of lower displacement from the set of 20 points (Fig. 3), the fitting algorithm adjusts the slope of a linear cohesive law in the numerical model to fit the experimental measurement. Once the error is less than a prescribed tolerance, the crack opening at the initial notch is read from the numerical model to provide the first segment of the cohesive law. Then, the procedure is repeated point by point to build a cohesive law with as many segments as experimental points that have been selected (20 in the present case).

3. $R(\Delta a)$ And $J(\omega)$ curves from OCT tests

Fig. 3 shows the experimental load displacement curves (solid lines) and the set of 20 representative points of each specimen (cross symbols) used for data reduction. The 20 points are distributed uniformly between the first point deviating from linearity and the onset point of other damage mechanisms (i.e., back end failure or buckling), as explained in Ortega et al. [43].

Fig. 4 exhibits the cohesive law for each of the OCT specimens in Fig. 3, obtained following the procedure described in the previous section.

Figs. 5a and 5b shows the R-curve of the laminates $[45, 90, -45, 0]_{4s}$ and $[90, 45, 0, -45]_{4s}$, respectively, while Figs. 5c and 5d the J curves resulting from the integration of the respective cohesive law.

The initial parts of the R-curves in Figs. 5a and 5b are similar to those deduced in a recent paper based on X-ray CT measurements of the crack length in the different sized OCT specimens [46].

3.1. Comparison of the $J(\omega)$ and the $R(\Delta a)$ curve

A remarkable fact is that while the J curves are almost independent of the specimen size, the R curves for small specimens are higher than for the other specimens. The explanation lies in the fact that the R curve approach can be applied only under the condition of a small non-linear zone compared to any other dimension of the specimen. This condition is more likely to be violated in tests on small specimens. ASTM [47,48] establishes a threshold for LEFM validity based on the expected size of the plastic zone: $G_C E/\sigma_u^2 < 0.4(W - a)$, as illustrated in Figs. 5a and 5b. This threshold is plausible for metals where the FPZ is indeed governed by plasticity with hardening. However, it underestimates the extension of the FPZ in materials with other constitutive equations, in particular, quasi-brittle materials [8]. In view of the independence of the J curve on the specimen size, this parameter provides a more objective measure of the fracture properties of the material. It appears that the small specimen limit is less restrictive or non-existent in the J curve characterization. This trend should be attributed to the idealization sketched in Fig. 1. In the cohesive zone model, the damaged length ℓ_H is explicitly considered and the only condition is that ℓ_V be small. This condition is very appropriate in materials with extrinsic dissipation mechanisms that tend to dissipate most of the energy in a localized region, such as laminated composites or concrete.

J and R, at the LEFM limit, define the same physical property [12] in spite of being determined through different procedures. Additionally, the J curve is expressed in terms of the crack opening and R in terms of the equivalent crack length. As a consequence, R usually starts at a finite value, the initiation toughness, while the J curve departs from origin (zero opening). One advantage of the $J(\omega)$ curve is that it can be easily implemented in finite element software with a user material cohesive law.

The comparison of the fracture properties of the two tested laminates, which have the same number of plies for each orientation and differ only on the stacking sequence (Table 1) illustrates how the cohesive law reflects the particular damage micromechanisms taking place in each material. The cohesive laws for both laminates and same specimen size, $W = 80.6$ mm (Fig. 6) are very similar for small crack openings, $\omega < 0.3$ mm, while they diverge afterwards. The cohesive law

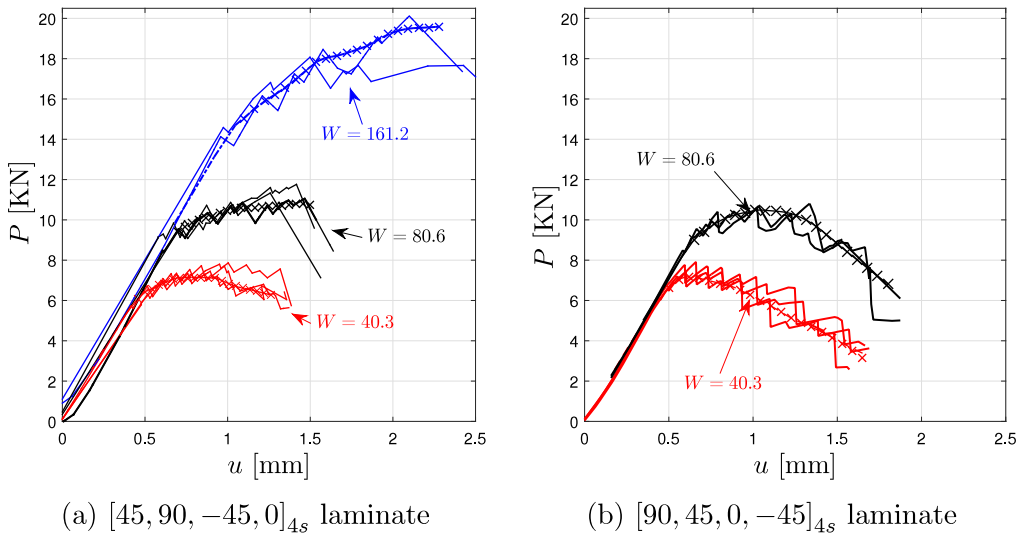

Fig. 3. Experimental load displacement curves and selected points to apply data reduction methods.

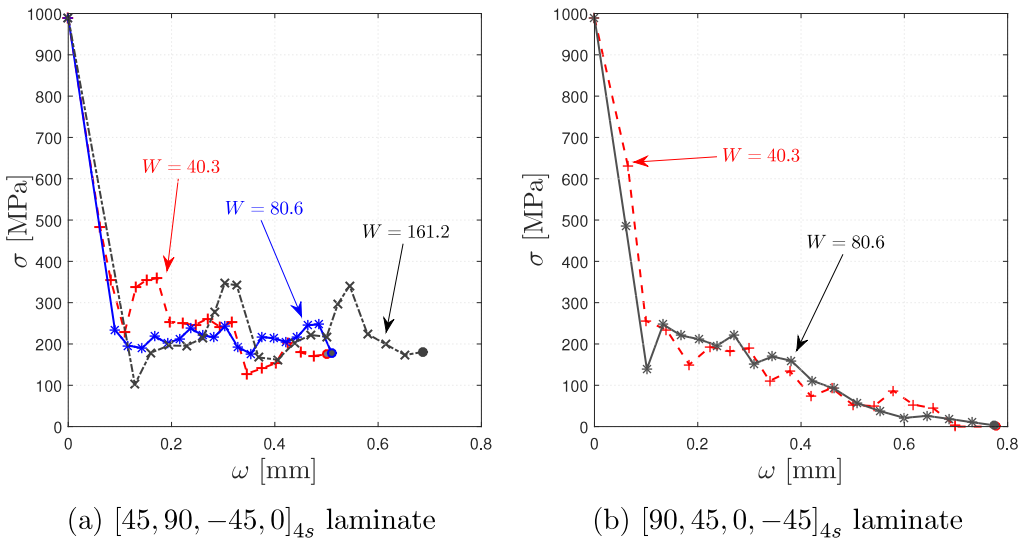

Fig. 4. Fitted translaminar traction separation law.

in the laminate $[45, 90, -45, 0]_{4s}$ is not fully determined because the FPZ could not develop entirely before the test ended. The reason being the cluster of 0^0 plies at the center of this laminate, which promotes the growth of splittings in the load direction and delamination in the adjacent plies, increasing the damage extension in the direction defined by ℓ_V. Nonetheless, it is remarkable how consistent the J-curves obtained for both laminates are, even in the presence of crack-splitting.

4. Predictive capability: Open hole and center cracked specimen strengths

Whether or not the $R(\Delta a)$ and $J(\omega)$ curves characterize the fracture behavior of the studied laminates, should be demonstrated by evaluating their predictive capability on specimens of different geometry than the one used to extract them. For that purpose, this section shows the prediction of the Open Hole (OH) and Center Cracked (CC) specimen strengths from the measured $R(\Delta a)$ and J -curves in the OCT experiments.

These predictions are compared against the nominal strength of geometrically similar CC and OH specimens presented for the laminate $[45, 90, -45, 0]_{4s}$ by Green et al. [18] and Xu et al. [19]. These authors tested a broad range of specimen sizes, with hole radii (OH), or half crack lengths (CC), a_0 = 1.5875, 3.175, 6.35, 12.7 and 25.4 mm. The a_0/b ratio was 0.2, b being the specimen width.

4.1. OH and CC strength from $J(\omega)$

Considering that the $J(\omega)$ curve is a material property, means that it is considered to develop similarly at any notch or stress raiser, independent of the specimen geometry.

We calculate the nominal strength of OH and CC specimens assuming a cohesive zone model following the approach presented in [49–51]. The cohesive law used is the mean cohesive law defined with the segments bounded by the points: $\sigma(\omega) = [990(0), 250(0.0893), 175(0.7)]$. The area below the curve is G_C = 185 N/mm up to ω = 0.7 mm. Fig. 7a shows the calculated ultimate net sectional stress for OH and CC geometrically similar specimens of different sizes, as well as the corresponding experimental results. It also includes the limit values for small and large specimens. For very small specimens, the response is notch insensitive and corresponds to the laminate strength σ_N = 990 MPa.

For large specimens, the CC strength tends to the LEFM limit, governed by G_C (taken as 185 N/mm, although it could be larger

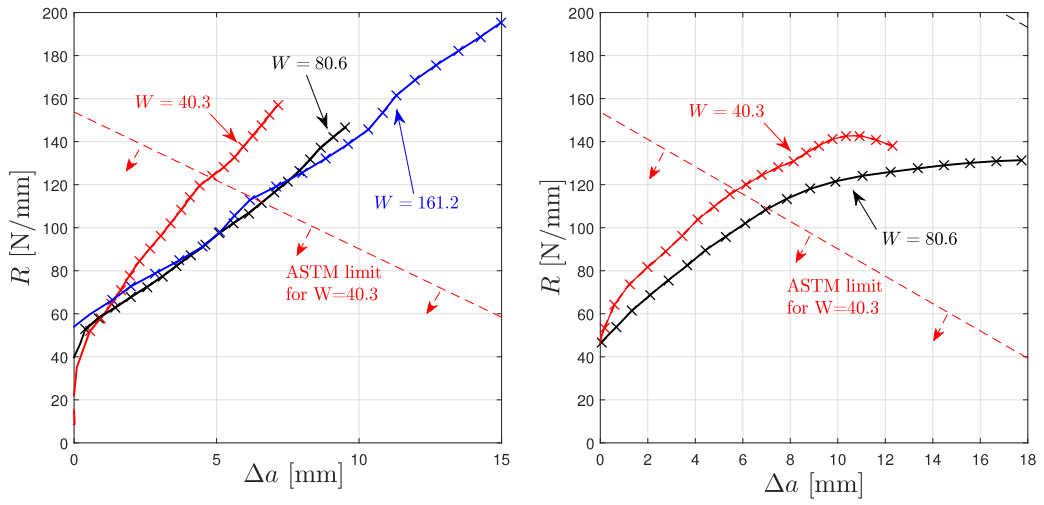

(a) R-curve of $[45, 90, -45, 0]_{4s}$ laminate (b) R-curve of $[90, 45, 0, -45]_{4s}$ laminate

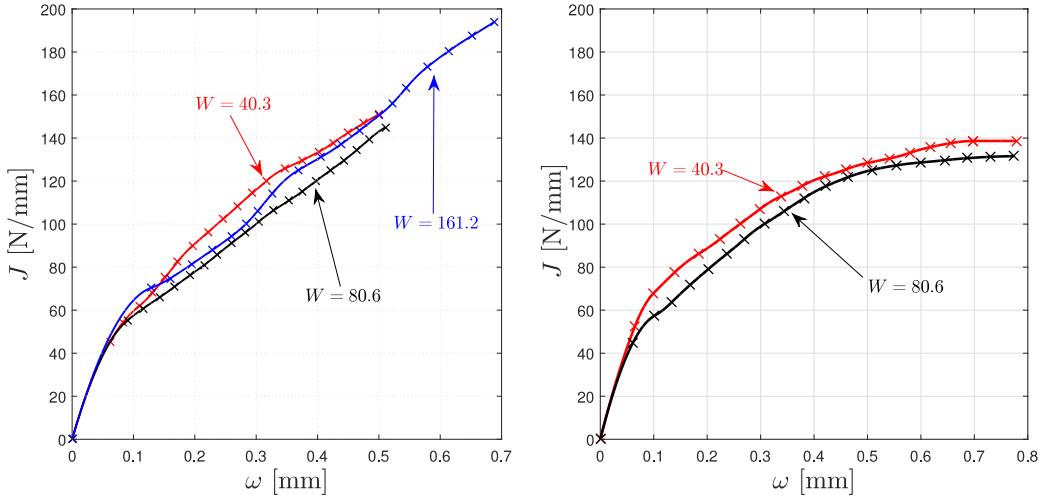

(c) J-curve of $[45, 90, -45, 0]_{4s}$ laminate (d) J-curve of $[90, 45, 0, -45]_{4s}$ laminate

Fig. 5. R and J-curves for the materials and sizes tested.

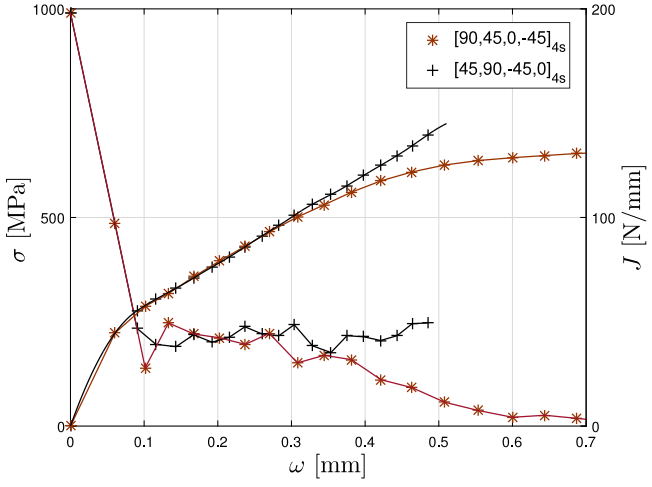

Fig. 6. Comparison of the CL and J curve for the two laminates. Responses for $W = 80.6$ mm.

because the cohesive law from which it is derived could not be entirely determined, Fig. 6 and Section 3.1), while the OH strength tends to the notch sensitivity response defined by the stress concentration factor $K_t = 2.53$ [52]; $\sigma_N = 391.3$ MPa

The calculation of the nominal strength of the CC specimen underpredicts the experimental results and slightly overpredicts those for OH. These results suggest that the nucleation and growth of the crack in the CC specimen requires more energy, and the OH less energy, than that represented by the $J(\omega)$ curve extracted from the OCT test. The source of this increment of dissipated energy is probably caused by different behavior of crack splitting at crack tip.

Fig. 7b displays the maximum crack opening at failure load (the crack opening at a_0) according to the cohesive zone model. For the OH specimen, the crack opening displacement is almost zero for large and small specimens. It reaches its maximum for hole radii between 2 and 3 mm. In any case, $\omega_{max} < 0.06$ mm for any hole radius. Taking into account that the kink point in the cohesive law of Fig. 4a is about 0.09 mm, the fact that $\omega_{max} < 0.06$ mm for any hole radius means that only the first part of the cohesive law is important to define the nominal strength of open hole specimens [50,51,53–55].

On the other hand, the maximum crack opening increases with specimen size for the CC specimens. Therefore, the first part of the

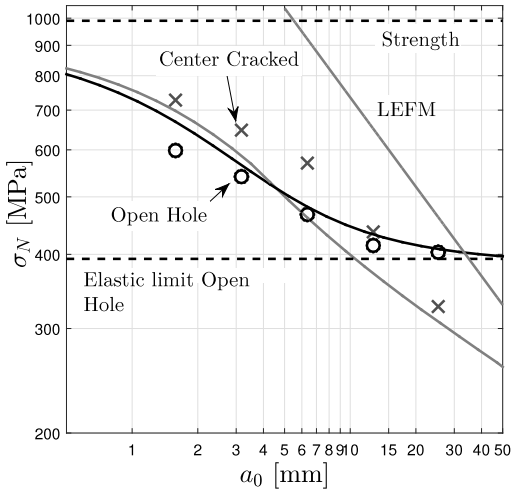

(a) Nominal strength.

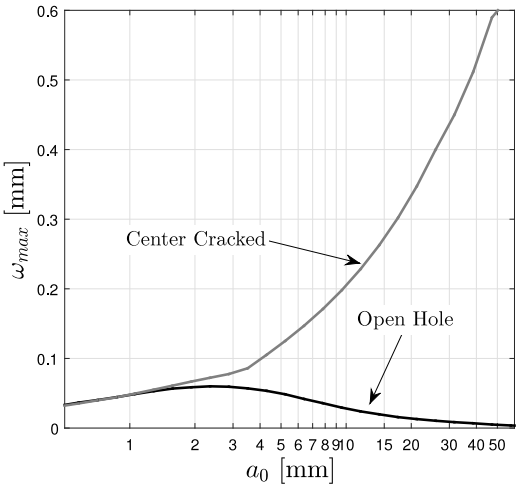

(b) Maximum crack opening displacement at failure load.

Fig. 7. Response of OH and CC for $[45, 90, -45, 0]_{4s}$ laminate.

cohesive law determines the strength in small specimens, whereas the complete cohesive law is involved in the fracture of large specimens. Consequently, the strength is defined by G_C, according to LEFM, in large specimens [51].

4.2. CC strength from $R(\Delta a)$

The R-curve alone does not allow for predicting the nominal strength of the OH specimens because it does not contain information on the material strength. Existing methods to obtain the notched strength by variations of the inherent flaw model or finite fracture mechanics [3,51,56,57] are outside the scope of this contribution.

The nominal strength of CC specimens has been estimated by considering the conditions for crack stability: $R = G$ and $dR/da = dG/da$. The expression for the Energy Release Rate, G of the CC specimen is [58]:

$$G = \frac{\sigma_N^2 b}{E} k^2 \quad \text{where} \quad k^2 = \pi(1-\bar{a}_0)^2 \bar{a} \sec(\pi \bar{a}/2) \tag{4}$$

where $\bar{a} = a/b$ and $\bar{a}_0 = a_0/b = 0.2$, b being the specimen width.

The nominal strength of the CC specimens computed by means of the R curve of each of the three tested OCT specimens ($W = 40.3, 80.6$ and 161.2 mm) is shown in Fig. 8. The calculations agree reasonably well with the experimental results although the calculations do not tend to the laminate strength for very small specimens.

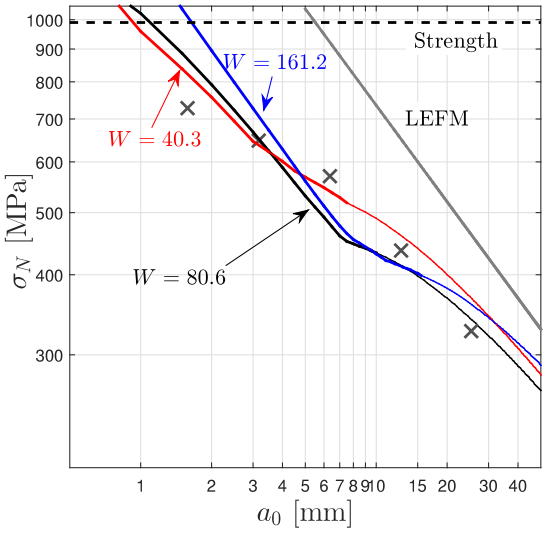

Fig. 8. Size effect law of CC specimen determined from the R-curve of the OCT specimens.

4.3. Characterization of fracture properties with center cracked specimen

As an additional analysis of the sensitivity of the strength of coupons of a particular geometry to the method used to determine the characteristic curves, $J(\omega)$ or $R(\Delta a)$, we find the cohesive law that betters fits the nominal strength of the OH and CC specimens, and the R curve that better fits the CC strength, the latter by means of the size effect law. Then, for example, the cohesive laws obtained in OCT experiments can be compared to the cohesive laws that better fit the nominal strength for OH and CC.

The curves of the nominal strength of OH and CC generated by means of the cohesive law derived from OCT tests are compared with the ones obtained by fitting in Fig. 9a. The cohesive laws for OH and CC determined by means of fitting appear in Fig. 9b, as well as those obtained from OCT tests. To find the cohesive law shape that better fits the experimental data, we used a numerical model as in Maimí et al. [50] and the shape of the cohesive law is changed to fit the experimental data. The cohesive law that better fits the nominal strength of OH specimens is defined by a straight line with a larger slope. Only the first part of the cohesive law can be determined because it is the only fraction that governs the strength of these specimens. On the other hand, the complete cohesive law can be determined from CC specimens provided that the specimen size is big enough which, in fact, is not practical. The cohesive law in CC specimens exhibits a smaller drop than the one found in the OCT tests. These results suggest that the damage mechanisms depend on the specimen geometry: splits are probably larger in cracked specimens than in open hole ones.

The R-curve can be derived from the nominal strength of CC specimens of different sizes following the size effect law proposed by Bažant et al. [8,59,60]. This has also been applied to edge cracked specimens of composite materials [61]. The R curve results from enforcing the conditions $R = G$ and $dR/db = dG/db = 0$ on specimens of different sizes; where b is a measure of the specimen size, in this case the specimen width. G is defined in Eq. (4). The nominal strength σ_N should be derived with respect to b, which can be done with the help

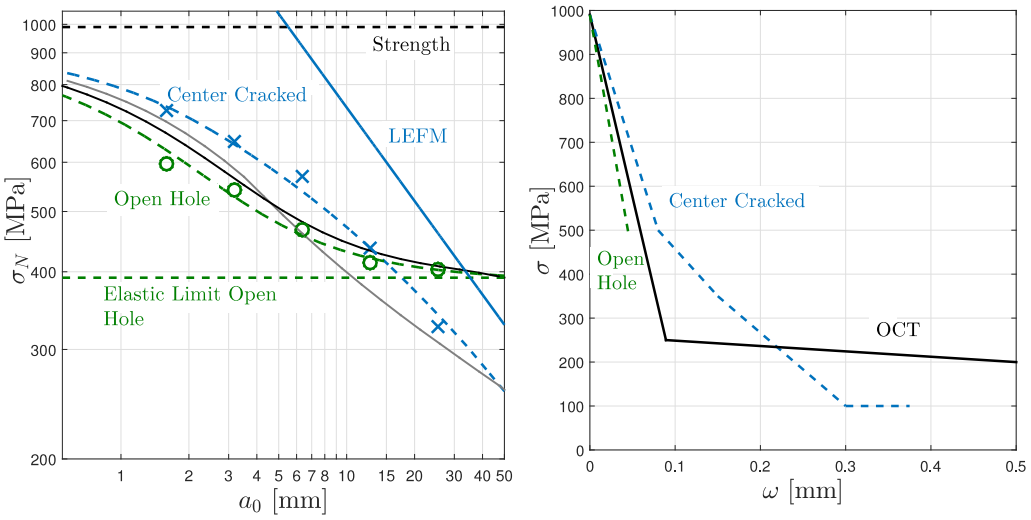

(a) Nominal strength (b) Cohesive laws

Fig. 9. Nominal strength of the Center Cracked and Open Hole specimens taking into account the cohesive law obtained with the OCT specimen (solid lines) and the optimal cohesive law (dotted lines).

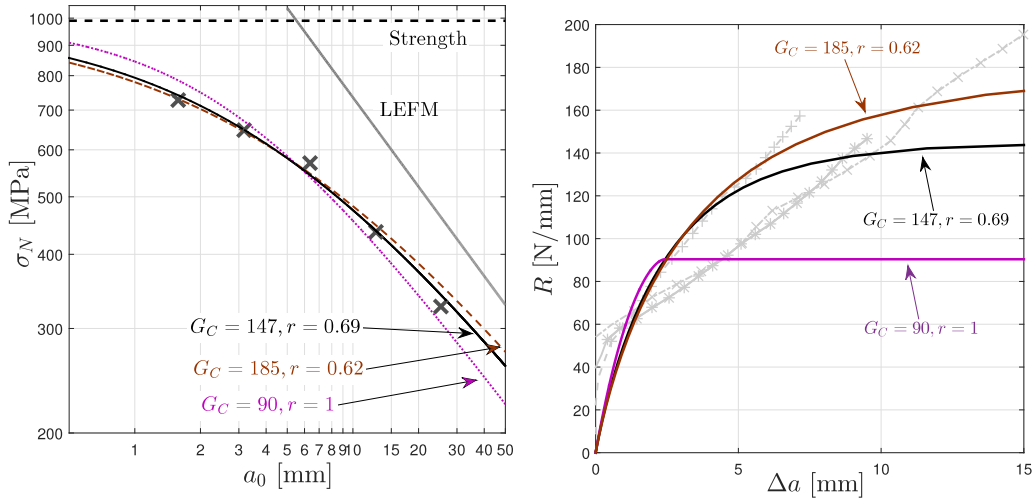

(a) Size effect law on the nominal strength (b) R-curve from the size effect law

Fig. 10. Nominal strength of the Center Cracked specimen and R-curves.

of the size effect law:

$$\sigma_N = \sigma_u \left(1 + \left(\frac{b}{b_0}\right)^r\right)^{\frac{-1}{2r}} \quad \text{where} \quad b_0 = \frac{EG_C}{k_0^2 \sigma_u^2} \tag{5}$$

The strength limit for small size specimens is determined by taking into account a notch insensitive response (i.e. $\sigma_N = \sigma_u$). G_C and r, the latter usually assumed to be 1, should be found by fitting the CC experimental data. We have performed three different fittings of the size effect law (Fig. 10a): (i) fixing $r = 1$ and searching G_C; (ii) setting G_C=185 N/mm and looking for r; and (iii) searching for both r and G_C. In all cases, σ_u=990 MPa as it results from an independent experiment. The R-curve is defined by the equations [8,59,60]:

$$\begin{aligned} \Delta a &= b_0 \left(\frac{k}{2k'(\bar{a}-\bar{a}_0)} - 1\right)^{\frac{1}{r}} (\bar{a} - \bar{a}_0) \quad \text{and} \\ R &= \left(2k^{2r-1} k' (\bar{a} - \bar{a}_0)^{1-r}\right)^{\frac{1}{r}} \frac{\Delta a}{k_0^2 b_0} \end{aligned} \tag{6}$$

The R curves corresponding to the three fittings are represented together with that from the OCT tests in Fig. 10b. The R curves from fitting tend to a steady value whereas the one obtained in the OCT tests grows continuously for the range of crack extension explored.

The main drawback of the determination of the R-curve by means of the size effect law is that it requires testing very large specimens to fit G_C properly. Determined by this method, the R-curve goes through the origin as the nominal strength for very small specimen is enforced, contrarily to the response determined from the OCT specimen shown in Fig. 8. The R-curve defined in this way is obviously independent on specimen size but it depends on specimen shape [8].

5. Conclusions

We have made use of a thorough experimental study on fracture specimens of laminated composites of different sizes published by other authors to investigate the suitability of the R curve and the cohesive law, taken as the J curve, to represent the fracture behavior of the tested materials at notches or stress raisers. Each of these curves emanate from a different theoretical frame: LEFM for R and cohesive zone models for the cohesive law / J curve.

The R and J curves were obtained from data reduction of the load–displacement curves of the Over-Height Compact Tension tests. Comparison of the results for scaled specimens showed that the R curves for small specimens deviate from the rest of the tests while J offers more consistent results. The R and J curves so deduced have been used to predict the nominal strength of OH and CC specimens as a predictive capability validation. Both curves, J and R, offer good predictions when computing the nominal strength of CC specimens. The R curve fails to reproduce the laminate strength for the CC small specimens while, for the analyzed material, J under-predicts the size effect of the CC specimens. Regarding the OH nominal strength, this can only be computed using J, as R does not encompass any information on the material strength. Using J, the size effect of the OH specimens was able to be captured correctly, although the numerical results tend to slightly over-predict the experimental results. The predictive capability of J should be considered as very positive, taking into account the difference in the stress raiser configuration between OCT (sharp notch) and OH (circular hole).

In a reverse effort, the cohesive laws for the CC and OH specimens were determined by fitting the experimental nominal strength data. This analysis revealed that the cohesive law is only slightly different for each specimen geometry. Finally, we determined the R curve by fitting the strength of the CC specimens to the size effect law. However, the determination of the fracture properties through the size effect law is expensive as it needs testing on large specimens to obtain the total fracture toughness. This limitation contrasts with using OCT specimens that only requires one specimen of appropriate size.

The paper evidences that methods based on the cohesive zone model better represent, and for a wider specimen size range, the fracture behavior of the explored laminated composites than the methods based on linear elastic fracture mechanics. The cause lies in the cohesive zone models assumptions being less restrictive than the LEFM hypothesis, thus permitting a better representation of the failure process zone. In spite of the increased complexity of the methods to obtain the cohesive law parameters (or the corresponding J curve), it appears to be the adequate methodology for fracture characterization of new engineered materials with high toughness, if very large specimens are to be avoided.

CRediT authorship contribution statement

P. Maimí: Conceptualization, Methodology, Writing – original draft. **A. Ortega:** Investigation, Software. **E.V. González:** Validation, Writing – review & editing. **J. Costa:** Methodology, Writing – review & editing.

Declaration of competing interest

The authors declare that they have no known competing financial interests or personal relationships that could have appeared to influence the work reported in this paper.

Acknowledgments

The financial support from the grant RTI2018-097880-B-I00 from the Spanish Ministerio de Ciencia, Innovación *y* Universidades is acknowledged. Open Access funding provided thanks to the CRUE-CSIC agreement with Elsevier.

References

[1] Xu X, Wisnom MR, Hallett SR. Deducing the R-curve for trans-laminar fracture from a virtual over-height compact tension (OCT) test. Composites A 2019;118(December 2018):162–70. http://dx.doi.org/10.1016/j.compositesa.2018.12.027.

[2] Whitney JM, Nuismer RJ. Stress fracture criteria for laminated composites containing stress concentrations. J Compos Mater 1974;8(3):253–65. http://dx.doi.org/10.1177/002199837400800303, URL http://jcm.sagepub.com/cgi/doi/10.1177/002199837400800303.

[3] Waddoups ME, Eisenmann JR, Kaminski B. Macroscopic fracture mechanics of advanced composite materials. J Compos Mater 1971;5:446–54.

[4] Tan SC. Effective stress fracture models for unnotched and notched multidirectional laminates. J Compos Mater 1988;22(4):322–40. http://dx.doi.org/10.1177/002199838802200402, URL http://jcm.sagepub.com/cgi/doi/10.1177/002199838802200402.

[5] Zok FW, Hom CL. Large scale bridging in brittle matrix composites. Acta Metall Mater 1990;38(10):1895–904. http://dx.doi.org/10.1016/0956-7151(90)90301-V.

[6] Suo Z, Bao G, Fan B. Delamination R-curve phenomena due to damage. J Mech Phys Solids 1992;40(1):1–16.

[7] Bao G, Suo Z. Remarks on crack bridging concepts. Appl Mech Rev 1992;45(8):355–66.

[8] Ortega A, Maimí P, González EV, Trias D. Specimen geometry and specimen size dependence of the R-curve and the size effect law from a cohesive model point of view. Int J Fract 2017;1–15. http://dx.doi.org/10.1007/s10704-017-0195-1.

[9] Kongshavn IA, Poursartip A. Experimental investigation of a strain-softening approach to predicting failure in notched fibre-reinforced composite laminates. Compos Sci Technol 1999;59(1):29–40. http://dx.doi.org/10.1016/S0266-3538(98)00034-7, URL http://linkinghub.elsevier.com/retrieve/pii/S0266353898000347.

[10] Barenblatt GI. The formation of equilibrium cracks during brittle fracture. General ideas and hypotheses. Axially-symmetric cracks. J Appl Math Mech 1959;23(3):622–36.

[11] Dugdale DS. Yielding of steel sheets containing slits. J Mech Phys Solids 1960;8(2):100–4.

[12] Rice JR. A path independent integral and approximate analysis of strain concentration by notches and cracks. J Appl Mech 1968;35(2):379.

[13] Ritchie RO. The conflicts between strength and toughness. Nature Mater 2011;10:817–22.

[14] Xu X, Wisnom MR, Mahadik Y, Hallett SR. Scaling of fracture response in over-height compact tension tests. Composites A 2015;69:40–8. http://dx.doi.org/10.1016/j.compositesa.2014.11.002.

[15] Zobeiry N, Vaziri R, Poursartip A. Characterization of strain-softening behaviour and failure mechanisms of composites under tension and compression. Composites A 2015;68:29–41. http://dx.doi.org/10.1016/j.compositesa.2014.09.009, URL http://linkinghub.elsevier.com/retrieve/pii/S1359835X14002826.

[16] Bergan A, Dávila CG, Leone FA, Awerbuch J, Tan T-M. A mode I cohesive law characterization procedure for through-the-thickness crack propagation in composite laminates. Composites B 2016;94:338–49. http://dx.doi.org/10.1016/j.compositesb.2016.03.071, URL http://linkinghub.elsevier.com/retrieve/pii/S1359836816301597.

[17] Médeau V, Laurin F, Rannou J, Hurmane A, Quillent H, Lachaud F. Robust characterization of crack propagation in 3D woven composites and evidences of size dependency. Compos Struct 2019;225(June):111175. http://dx.doi.org/10.1016/j.compstruct.2019.111175.

[18] Green BG, Wisnom MR, Hallett SR. An experimental investigation into the tensile strength scaling of notched composites. Composites A 2007;38(3):867–78. http://dx.doi.org/10.1016/j.compositesa.2006.07.008, URL http://www.sciencedirect.com/science/article/pii/S1359835X06002326.

[19] Xu X, Wisnom MR, Mahadik Y, Hallett SR. An experimental investigation into size effects in quasi-isotropic carbon/epoxy laminates with sharp and blunt notches. Compos Sci Technol 2014;100:220–7. http://dx.doi.org/10.1016/j.compscitech.2014.06.002.

[20] Kongshavn IA. Experimental investigation of a strain softening approach to predicting failure of notched composite laminates. 1996.

[21] Floyd AM. An engineering approach to the simulation of gross damage development in composite laminates (Ph.D. thesis), The University of British Columbia; 2004.

[22] Li X, Hallett SR, Wisnom MR, Zobeiry N, Vaziri R, Poursartip A. Experimental study of damage propagation in over-height compact tension tests. Composites A 2009;40(12):1891–9. http://dx.doi.org/10.1016/j.compositesa.2009.08.017, URL http://linkinghub.elsevier.com/retrieve/pii/S1359835X09002553.

[23] Ortega A, Maimí P, González EV, Ripoll L. Compact tension specimen for orthotropic materials. Composites A 2014;63:85–93. http://dx.doi.org/10.1016/j.compositesa.2014.04.012, URL http://linkinghub.elsevier.com/retrieve/pii/S1359835X14001146.

[24] Xu X, Wisnom MR, Chang K, Hallett SR. Unification of strength scaling between unidirectional, quasi-isotropic, and notched carbon/epoxy laminates. Composites A 2016;90:296–305. http://dx.doi.org/10.1016/j.compositesa.2016.07.019.

[25] Laffan M, Pinho ST, Robinson P, Iannucci L. Measurement of the in situ ply fracture toughness associated with mode I fibre tensile failure in FRP. Part I: Data reduction. Compos Sci Technol 2010;70(4):606–13. http://dx.doi.org/10.1016/j.compscitech.2009.12.016, URL http://linkinghub.elsevier.com/retrieve/pii/S0266353809004515.

[26] Maimí P, Wagih A, Ortega A, Xavier J, Blanco N, Ponces Camanho P. On the experimental determination of the J-curve of quasi-brittle composite materials. Int J Fract 2020;224(2):199–215. http://dx.doi.org/10.1007/s10704-020-00456-0.

[27] Cherepanov GP. Crack propagation in continuous media. J Appl Math Mech 1967;31(3):476–88. http://dx.doi.org/10.1016/0021-8928(67)90034-2.
[28] Roelfstra PE, Wittmann FH. Fracture toughness and fracture energy of concrete engineering. In: Wittmann, editor. Fracture toughness and fracture energy of concrete. Elsevier; 1986, p. 163–75, (Ch. Numerical).
[29] Yang QD, Thouless MD, Ward SM. Numerical simulations of adhesively-bonded beams failing with extensive plastic deformation. J Mech Phys Solids 1999;47(6):1337–53. http://dx.doi.org/10.1016/S0022-5096(98)00101-X.
[30] Yang C, Tomblin JS. Investigation of adhesive behavior in aircraft applications. Tech. rep., Washington: Office of Aviation Research; 2001, p. 52, September.
[31] Wittmann F, Rokugo K, Brühwiler E, Mihashi H, Simonin P. Fracture energy and strain softening of concrete as determined by means of compact tension specimens. Mater Struct 1988;21(1):21–32. http://dx.doi.org/10.1007/BF02472525.
[32] Bolzon G, Maier G. Identification of cohesive crack models for concrete on the basis of three-point-bending tests. In: Computational modelling of concrete structures. 1988, p. 301–8.
[33] Ulfkjær JP, Brincker R. Indirect determination of the sigma - omega relation of HCS through three-point bending. Tech. rep., Aalborg: Dept. of Building Technology and Structural Engineering, Aalborg University; 1992.
[34] Guinea GV, Planas J, Elices M. A general bilinear fit for the softening curve of concrete. Mater Struct 1994;27(2):99–105, URL http://www.scopus.com/inward/record.url?eid=2-s2.0-0028399561&partnerID=40.
[35] Kitsutaka Y. Fracture parameters by polylinear tension-softening analysis. J Eng Mech 1997;123(5):444–50. http://dx.doi.org/10.1061/(ASCE)0733-9399(1997)123:5(444).
[36] Tin-Loi F, Que NS. Parameter identification of quasibrittle materials as a mathematical program with equilibrium constraints. Comput Methods Appl Mech Engrg 2001;190(43–44):5819–36. http://dx.doi.org/10.1016/S0045-7825(01)00199-2, URL http://linkinghub.elsevier.com/retrieve/pii/S0045782501001992.
[37] Que NS, Tin-Loi F. An optimization approach for indirect identification of cohesive crack properties. Comput Struct 2002;80(16–17):1383–92. http://dx.doi.org/10.1016/S0045-7949(02)00096-2, URL http://www.sciencedirect.com/science/article/pii/S0045794902000962.
[38] Bolzon G, Fedele R, Maier G. Parameter identification of a cohesive crack model by Kalman filter. Comput Methods Appl Mech Engrg 2002;191(25–26):2847–71. http://dx.doi.org/10.1016/S0045-7825(02)00223-2, URL http://www.sciencedirect.com/science/article/pii/S0045782502002232.
[39] Tin-Loi F, Que NS. Identification of cohesive crack fracture parameters by evolutionary search. Comput Methods Appl Mech Engrg 2002;191(49–50):5741–60. http://dx.doi.org/10.1016/S0045-7825(02)00483-8, URL http://www.sciencedirect.com/science/article/pii/S0045782502004838.
[40] Luiz J, Oliveira AD, Gettu R. Determining the tensile stress-crack opening curve. J Eng Mech 2006;132(2):141–8.
[41] Dourado N, De Moura MFSF, De Morais AB, Pereira AB. Bilinear approximations to the mode II delamination cohesive law using an inverse method. Mech. Mater. 2012;49:42–50. http://dx.doi.org/10.1016/j.mechmat.2012.02.004.
[42] Silva FGA, Morais JJL, Dourado N, Xavier J, Pereira FAM, De Moura MFSF. Determination of cohesive laws in wood bonded joints under mode II loading using the ENF test. Int J Adhes Adhes 2014;51(8):54–61. http://dx.doi.org/10.1016/j.ijadhadh.2014.02.007.
[43] Ortega A, Maimí P, González EV, Trias D. Characterization of the translaminar fracture cohesive law. Composites A 2016;91:501–9. http://dx.doi.org/10.1016/j.compositesa.2016.01.019.
[44] Ortega A, Maimí P, González EV, Sainz de Ajá J, Martín de la Escalera F, Cruz P. Translaminar fracture toughness of interply hybrid laminates under tensile and compressive loads. Compos Sci Technol 2017;143. http://dx.doi.org/10.1016/j.compscitech.2017.02.029, URL http://linkinghub.elsevier.com/retrieve/pii/S0266353816318243.
[45] Pereira FA, de Moura MF, Dourado N, Morais JJ, Xavier J, Dias MI. Direct and inverse methods applied to the determination of mode I cohesive law of bovine cortical bone using the DCB test. Int J Solids Struct 2017;128:210–20. http://dx.doi.org/10.1016/j.ijsolstr.2017.08.028.
[46] Xu X, Sun X, Wisnom MR. Initial R-curves for trans-laminar fracture of quasi-isotropic carbon / epoxy laminates from specimens with increasing size. Compos Sci Technol 2021;216(July):109077. http://dx.doi.org/10.1016/j.compscitech.2021.109077.
[47] ASTM E 399. Standard test method for linear-elastic plane-strain fracture toughness KIc of metallic materials. 2009.
[48] ASTM D 5045. Standard test methods for plane-strain fracture toughness and strain energy release. 1999, p. 1–9.
[49] Soutis C, Fleck NA, Smith PA. Failure prediction technique for compression loaded carbon fibre-epoxy laminate with open holes. J Compos Mater 1991;25(11):1476–98.
[50] Maimí P, Trias D, González EV, Renart J. Nominal strength of quasi-brittle open hole specimens. Compos Sci Technol 2012;72(10):1203–8. http://dx.doi.org/10.1016/j.compscitech.2012.04.004.
[51] Maimí P, González EV, Gascons N, Ripoll L. Size effect law and critical distance theories to predict the nominal strength of quasibrittle structures. Appl Mech Rev 2013;65(2):20802. http://dx.doi.org/10.1115/1.4024163.
[52] Pilkey WD, Pilkey DF. Peterson's stress concentration factors. John Wiley and Sons Inc; 2008, p. 560.
[53] Kabeel AM, Maimí P, Gascons N, González EV. Nominal strength of quasi-brittle open hole specimens under biaxial loading conditions. Compos Sci Technol 2013;87:42–9. http://dx.doi.org/10.1016/j.compscitech.2013.07.022, URL http://linkinghub.elsevier.com/retrieve/pii/S0266353813002960.
[54] Kabeel AM, Maimí P, Gascons N, González EV. Net-tension strength of double lap joints taking into account the material cohesive law. Compos Struct 2014;112:207–13. http://dx.doi.org/10.1016/j.compstruct.2014.02.008, URL http://linkinghub.elsevier.com/retrieve/pii/S026382231400066X.
[55] Kabeel AM, Maimí P, González EV, Gascons N. Net-tension strength of double-lap joints under bearing-bypass loading conditions using the cohesive zone model. Compos Struct 2015;119:443–51. http://dx.doi.org/10.1016/j.compstruct.2014.08.036, URL http://linkinghub.elsevier.com/retrieve/pii/S0263822314004267.
[56] Leguillon D. Strength or toughness? A criterion for crack onset at a notch. Eur J Mech A Solids 2002;21(1):61–72. http://dx.doi.org/10.1016/S0997-7538(01)01184-6, URL http://www.sciencedirect.com/science/article/pii/S0997753801011846.
[57] Furtado C, Arteiro A, Bessa MA, Wardle BL, Camanho PP. Prediction of size effects in open-hole laminates using only the Young's modulus, the strength, and the R-curve of the 0 ply. Composites A 2017;101:306–17. http://dx.doi.org/10.1016/j.compositesa.2017.04.014.
[58] Tada H, Paris PC, Irwin GR. The stress analysis of cracks handbook. New York: American Society of Mechanical Engineers; 2000, p. 696.
[59] Bažant ZP, Kim J-k, Pfeiffer PA. Continuum model for progressive cracking and identification of nonlinear fracture parameters. In: Shah SP, editor. Application of fracture mechanics to cementitious composites. Dordrecht-Boston: Martinus Nijhoff Publishers; 1984, p. 197–246.
[60] Bažant ZP, Planas J. Fracture and size effect in concrete and other quasibrittle materials. CRC Press; 1998, p. 616.
[61] Catalanotti G, Arteiro a, Hayati M, Camanho PP. Determination of the mode I crack resistance curve of polymer composites using the size-effect law. Eng Fract Mech 2013;118:49–65. http://dx.doi.org/10.1016/j.engfracmech.2013.10.021, URL http://linkinghub.elsevier.com/retrieve/pii/S0013794413003640.